MLS Ice Water Content and Horizontally Finite Clouds

James Hocking, Dr Cory Davis

***Abstract*—An analysis of uncertainties in retrievals of ice water content (IWC) from the Earth Observing System (EOS) Microwave Limb Sounder (MLS) on the NASA Aura satellite is described. Errors in IWC retrievals due to variability in cloud shape and size, and in the relative position of cloud and sensor are investigated through analysis of data from simulations of MLS observations of high-altitude clouds. These errors are found to be of the same magnitude as estimated errors based on comparison of EOS MLS IWC with CloudSat IWC retrievals for observations at 147 hPa, while at 100 and 215 hPa the estimated errors are respectively smaller and larger than the CloudSat estimates. The errors due to assumptions regarding the particle size distribution are also considered and are found to be potentially much larger than those due to geometrical factors, especially for observations at higher tangent heights. Retrieval of the total ice mass within the instrument field-of-view is also considered and uncertainties in this quantity are found to be broadly comparable to uncertainties in IWC. Ice mass is an additional cloud parameter which may be retrieved from MLS measurements.**

***Index Terms*—Ice water content (IWC), limb sounding, microwave, satellite, upper-tropospheric clouds.**

I. Introduction

UPPER-TROPOSPHERIC (UT) clouds persistently cover around 20% of the sky and as such play a critical role in the Earth's climate [1]. Despite their ubiquity they are relatively poorly understood. For example, the net effect of cirrus clouds on the radiation budget is unknown: cirrus clouds act both to warm the Earth by absorbing outgoing long-wave terrestrial radiation, and to cool the planet by reflecting short-wave solar radiation back into space. Determining which of these two effects is larger requires knowledge of the microphysical properties of the clouds, a key one of which is ice water content (IWC) [2].

IWC of UT clouds is a product offered by the Earth Observing System (EOS) Microwave Limb Sounder (MLS) derived from data from its 240 GHz radiometer [3]. At large tangent heights the MLS line of sight (LOS) penetrates the entire atmospheric limb. When clouds are present, thermal radiation is scattered by ice particles into the LOS of the sensor and the ice particles themselves emit radiation. These processes cause an increase in measured limb radiances as compared to observations made of clear sky. This cloud-induced radiance (the difference between cloudy- and clear-sky radiances, denoted T_{cir}) is approximately proportional to the IWC and allows IWC to be derived from MLS measurements. The retrieved IWC represents an average over a sampling volume $\sim 300 \times 7 \times 4$ km^3 in the along-track, across-track and vertical directions, centred at the tangent point along the sensor LOS. The current method for retrieving IWC from MLS measurements provides coefficients for the relationship between T_{cir} and IWC at altitudes between 215 and 68 hPa which allow fast retrievals of IWC from MLS measurements [3]. The retrieved IWC show good agreement with existing Global Circulation Models (GCMs) [4]. However, the simulations used to obtain these coefficients were based on a one-dimensional atmospheric model: the cloud layer was assumed to be horizontally infinite with uniform thickness. The simulations therefore did not provide an estimate of the error in retrieved IWC values due to variability in the horizontal extent of clouds and the relative positioning of cloud and sensor. Cirrus clouds vary widely in terms of shape and altitude ([5]) and so measurements of T_{cir} made in the presence of different clouds of a particular IWC may be expected to show variability also.

This paper presents the results of an investigation into the uncertainty in EOS MLS IWC retrievals based on the analysis of results from three-dimensional simulations of MLS observations of UT clouds. Section II describes the simulation parameters and Section III discusses how IWC is defined. The estimated uncertainties in the measurements due to horizontal inhomogeneity and relative cloud-sensor position are presented in Section IV, while Section V examines how the choice of particle size distribution affects the IWC retrievals. Section VI considers retrieval of the total ice mass within the field-of-view (FOV), and is followed by a summary of the findings.

II. Simulation Methodology

Simulations were carried out using the Atmospheric Radiative Transfer Simulator (ARTS) [6]. ARTS is an open-source, modular software package created for use in modelling radiative transfer for millimetre and sub-millimetre remote sensing. Recently incorporated into ARTS is ARTS-MC, a three-dimensional radiative transfer model developed in order to assess the influence of cirrus cloud on satellite observations [7].

For this study, each ARTS simulation consisted of a cloud modelled as a cuboid (known as the cloud box) containing a specified distribution of ice particles, fields for key atmospheric parameters and constituents, and sensors with specified positions and lines-of-sight. Fig. 1 illustrates a typical scenario.

The goal was to generate scenarios randomly, performing Monte Carlo-style sampling of MLS observations in order to measure the uncertainty in retrieved IWC. The simulation parameters were chosen to be representative of tropical latitudes and were chosen on the basis of existing studies of tropical cirrus characteristics as described in the following sections.

A. Cloud dimensions

In collating a wide range of observations of cirrus, Dowling and Radke [5] found that ice cloud depths (vertical extent) varied between 0.1 km and 8 km with a mean depth of 1.5 km. Cloud altitudes were found to vary between 4 and 20 km, with a mean cloud-centre altitude at approximately 75% of the height of the tropopause ($\sim$13 km near the equator). The horizontal extent of cirrus clouds varies from tens to hundreds (or even thousands) of kilometres. The dimensions of the cloud box for each simulation were selected as follows:

- the altitude of the base of the cloud was chosen randomly between 10 and 17 km
- the depth of the could was chosen randomly such that it lay between 1 km and 18 km minus the altitude
- the horizontal extent of the cloud in both directions was chosen randomly between 20 and 800 km.

Clouds thus occupied heights between 10 and 18 km with depths of 1 to 8 km depending on altitude. By picking altitude followed by depth (as a function of altitude) and sampling cloud shapes uniformly within this "depth-altitude" space, more thin clouds were generated than thick clouds. This broadly matches the observations reported by Dowling and Radke, though the mean depth was $\sim$3.5 km, larger than the 1.5 km cited by Dowling and Radke. The cloud width was picked from a uniform distribution and the widest clouds filled the entire region of the troposphere through which the MLS LOS would pass in the case where the tangent point is at the centre of the cloud.

B. Cloud ice particles

It is understood that ice particles in cirrus clouds come in a wide variety of shapes (e.g. [8]). Particles were modelled as spheres under the assumption that the scattering properties of spherical particles with an appropriate distribution of particle sizes would not differ greatly from actual cloud particles when averaged over an entire cloud.

The distribution of particle sizes within cirrus clouds is a subject of much research and appears to be very variable. The assumed particle size distribution (PSD) has a large impact on IWC retrievals. The larger particles within the cloud contribute most of the scattered radiation at 240 GHz, while the smallest particles are effectively invisible as they are much smaller than the wavelength of the radiation. A PSD defines how the amount of ice mass within the cloud is divided between larger and smaller particles, and hence determines the total IWC that will be associated with a given observed radiance. Initially, the PSD chosen was that described by McFarquhar and Heymsfield [9] (henceforth denoted MH97) which is based on aircraft measurements in sub-tropical clouds. This PSD is a function of temperature and IWC, and consists of two modes, one each for small and large particles. It was used to derive the existing retrieval coefficients [3]. In that study it was found that employing alternative PSD parameterisations resulted in significantly different values of retrieved IWC. In order to gain insight into the sensitivity of the retrievals to choice of size distribution, simulations were also run with alternative PSDs: the bimodal distribution described by Mitchell *et al.* [10] (M99),

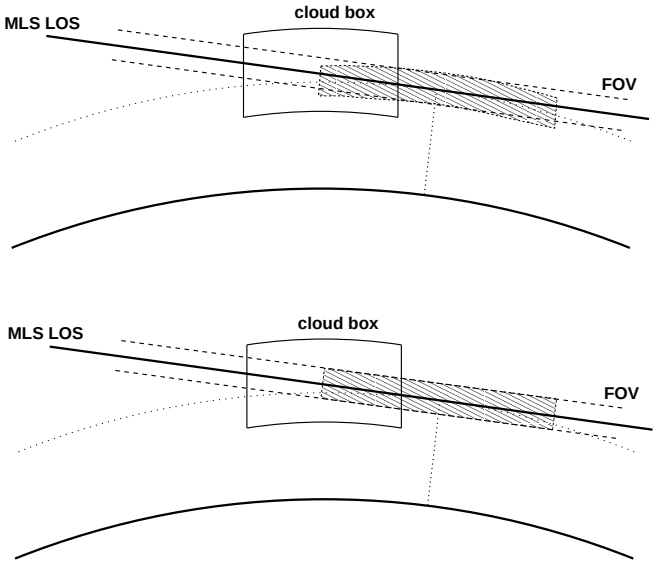

Fig. 1. Schematic diagram illustrating a simulation scenario. Sampling volumes are indicated by the hatched regions: EOS MLS IWC is defined over the EOS sampling volume which is parallel to the ground (top), while an alternative definition is the LOS sampling volume, parallel to the LOS (bottom). IWC is calculated as the ice mass in the intersection between the sampling volume and the cloud box averaged over the sampling volume.

and the unimodal gamma distribution described by Heymsfield [11] (H03). For H03 the parameters of the distribution were randomised to carry out Monte Carlo sampling of PSD as well as the other simulation parameters. Further discussion of the size distributions is reserved for Section V.

IWC within clouds has been found to vary approximately exponentially with temperature. For example, Bond [12] calculates an exponential best-fit for IWC versus temperature based on an analysis by Heymsfield and Platt [13], although these measurements were of mid-latitude frontal cirrus. Heymsfield and McFarquhar compare values of IWC at different temperatures from a range of studies of tropical clouds [14]. The findings display a large variance making it difficult to characterise the distribution accurately. Broadly speaking, IWC values are found to be of order 1-10 mg/m^3 at $\sim -70\,^\circ$C and of order 10-100 mg/m^3 at $\sim -40\,^\circ$C. Considering a difference of one order of magnitude between these two temperatures gives a crude approximation to the distribution of IWC with temperature: IWC $\propto e^{0.077T}$ where T is the temperature in Kelvin. The IWC field within the cloud box followed this distribution with temperature. Each cloud was assigned an overall average IWC value at random in the range 1-150 mg/m^3, and the distribution was scaled appropriately.

C. Atmospheric fields

Retrievals of IWC use a window channel of the 240 GHz radiometer, so the most relevant atmospheric constituents are N_2, O_2, and H_2O. Profiles for concentrations of these molecules and for atmospheric pressure, temperature and corresponding geometric height were taken from the FASCOD data for equatorial latitudes [15].

Within cirrus clouds the air is typically supersaturated with respect to ice. The H_2O profile within the cloud box was

TABLE I
SAMPLING VOLUME: ALONG-TRACK, ACROSS-TRACK AND VERTICAL EXTENTS

Pressure (hPa)	Dimensions (km)
100	$200 \times 7 \times 5$
147	$300 \times 7 \times 4$
215	$300 \times 7 \times 4$

therefore set to a random relative humidity over ice (RHI) of between 100% and 160%, the probability of a given RHI being proportional to $e^{-11.5\mathrm{RHI}}$. This broadly approximates the distribution of RHI observed in cirrus clouds, shown in Fig. 2 of [16]. No attempt was made to approximate the H_2O concentrations found outside, but near to, cirrus clouds. The relative humidity was found to have a comparatively small effect on the observed radiances (less than 2 K).

D. Sensor parameters

IWC measurements are made using data from the MLS 240 GHz radiometer. This is a double-sideband receiver in which signals measured are the sum from the two sidebands. A window channel is used for IWC retrieval in order to minimise the effects of molecular absorption in the atmosphere. The frequencies of this channel are 232.5 and 246.8 GHz. For the simulations, the antenna sensitivity pattern was modelled with a two-dimensional Gaussian function based on the MLS antenna characteristics given in [17].

IWC can be retrieved from MLS measurements at tangent heights between 215 and 68 hPa (roughly 12 to 18 km at the equator) [3]. For each cloud, sensors were placed at the altitude of the EOS MLS instrument (705 km) with LOS at tangent heights of 215, 147 and 100 hPa. Sensor position and LOS were determined by randomly selecting a value for the horizontal distance between the tangent point of the LOS and the centre of the cloud box. The only requirement was that the instrument FOV intersect the cloud box since otherwise the scenario would represent a clear-sky observation. This includes scenarios in which the sampling volume and cloud box do not intersect (giving zero IWC) while the LOS passes through the cloud giving significant observed radiance. This has implications for the uncertainty in the IWC retrievals as discussed in the next section.

A large number of scenarios were generated with approximately 1000 data points collected at each tangent height. In each one the simulated clear-sky radiance at the corresponding tangent height was subtracted from the simulated observed radiance to obtain the cloud-induced radiance for each sensor. The estimated error in each simulated radiance was less than 0.5 K. This is comparable with errors in measurements from the 240 GHz MLS radiometer [18].

III. DEFINITION OF IWC

EOS MLS IWC retrievals are taken to represent averages over a sampling volume centred at the tangent point along the LOS. Table I shows the dimensions of the sampling volume as defined in [19]. For EOS IWC measurements, the sampling volume is defined to be parallel to the ground as shown in Fig. 1. This will henceforth be denoted the EOS sampling volume (SV). The antenna sensitivity pattern exhibits symmetry about the LOS, so a plausible alternative definition has the sampling volume parallel to the LOS (Fig. 1, denoted LOS SV). For each scenario, the IWC was calculated as the ice mass in the intersection between the sampling volume and the cloud box averaged over the sampling volume for both of these definitions. A key source of uncertainty in these measurements arises from situations where the LOS passes through the cloud and the cloud box and sampling volume are disjoint. This can happen when the tangent point lies sufficiently far from the centre of the cloud, and also at low tangent heights when the cloud layer exists entirely above the sampling volume. The latter occurs more frequently with the EOS SV and so more zero IWC data points were found with this definition. The result is a zero (or very low) IWC corresponding to significant T_{cir}, and this can lead to a considerable over-estimate of the true IWC within the sampling volume. The effect is observed in Fig. 2 which plots T_{cir} against EOS sampling volume IWC for simulated measurements at 215 hPa. It can be seen that for T_{cir} up to ∼90 K, there are scenarios in which the associated IWC is zero.

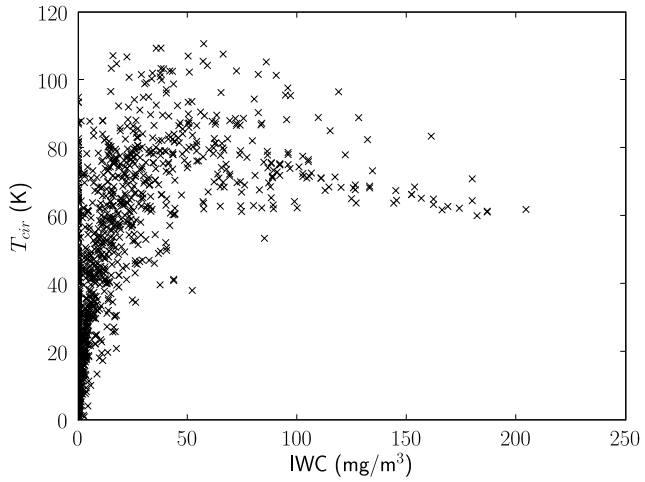

Fig. 2. T_{cir} against average IWC within the EOS SV for observations at 215 hPa. The saturation effect is observed for $T_{cir} > 60$ K.

In general, all of the ice mass within the FOV contributes to the observed radiance. This excludes circumstances where there is sufficient ice mass for the cloud to become opaque, in which case ice mass on the far side of the cloud from the sensor is obscured from the view of the sensor. This saturation effect can be seen in Fig. 2 for $T_{cir} > 60$ K where the variance in IWC quickly becomes very large indeed. This effectively places an upper limit on the values of T_{cir} which can usefully predict IWC.

Since ice mass along the entire LOS scatters radiation towards the sensor, it is reasonable to ask whether the average IWC of the cloud within the whole FOV can be more accurately predicted by T_{cir}. This is not the case as Fig. 3 shows. Here the IWC is calculated by averaging the total ice mass in the FOV over the volume of the intersection of the FOV

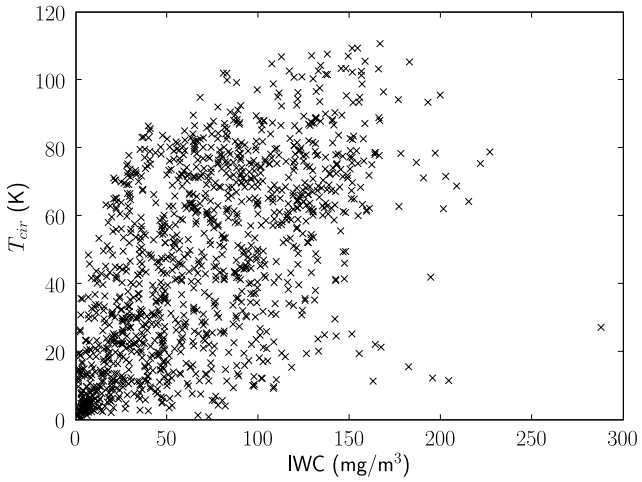

Fig. 3. T_{cir} against average IWC within the total FOV for observations at 215 hPa. Here IWC is calculated as the total ice mass within the FOV averaged over the volume of the intersection between the FOV and the cloud box. T_{cir} is a poor predictor of this measure of IWC.

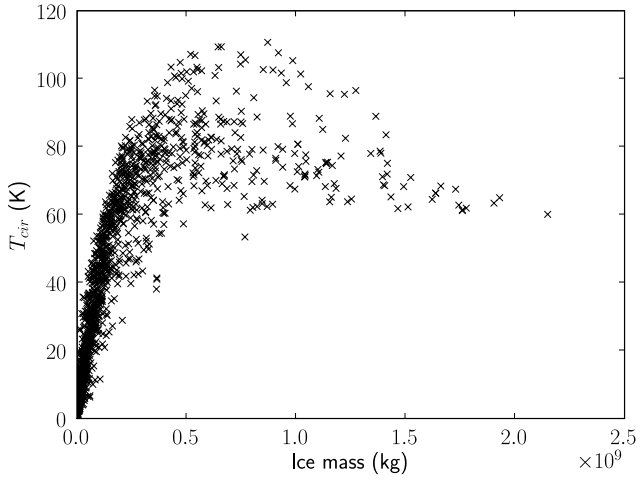

Fig. 4. T_{cir} against ice mass within the total FOV for observations at 215 hPa. There appears to be a strong correlation between T_{cir} and ice mass until the saturation effect occurs.

and the cloud box. The dimensions of the FOV are the same as those for the sampling volume across the LOS, but this volume extends all the way along the LOS (Fig. 1). The large spread of IWC values shows that T_{cir} is a poor predictor of this measure of IWC. The large variance is due to the fact that T_{cir} provides no indication of how the ice mass is distributed along the LOS: an extensive cloud of low ice density can yield the same T_{cir} as a small cloud of higher density.

Fig. 4 shows total ice mass in the FOV against T_{cir} and it can be seen that for lower values of the ice mass there appears to be a strong correlation between the two variables. This suggests that the total ice mass along the LOS may be inferred from cloud induced radiance, perhaps with greater accuracy than IWC, so long as the saturation level is not exceeded. The following sections analyse the relationship between IWC and T_{cir}, and between ice mass and T_{cir}.

IV. Horizontally Finite Clouds

A. Least-squares IWC-T_{cir} models

Least-squares lines of best-fit were applied to the simulated data in order to calculate the estimated uncertainty in IWC retrievals at 215, 147 and 100 hPa. At the two lower altitudes the saturation effect is observed for high T_{cir}. At 215 hPa, the variance in IWC increases sharply for $T_{cir} > 60$ K so samples with radiance above this limit were excluded from the error analysis. The cut-off at 147 hPa occurs at approximately the same point, though the increase in variance in IWC is less sharp than at 215 hPa. For 100 hPa the saturation effect is not clearly in evidence. The data were limited to $T_{cir} < 80$ K in order to exclude the small number of points above this level, some of which appeared to be outliers, possibly indicating saturation. The fact that the saturation effect is not clearly observed at 100 hPa is probably due to the assumption that IWC varies exponentially with temperature: IWC values were generally much smaller at this tangent height than the other two. In addition, at lower temperatures the ice mass comprises a smaller proportion of larger particles (as defined by the particle size distribution). This means there are fewer scattering particles for any given IWC at higher altitude, and hence saturation will occur for higher IWC than at lower altitude.

The simulated data do not follow the linear relationships derived by Wu *et al.* [3]. This is perhaps to be expected as a result of the significant differences between the parameters of the those simulations and the current ones. In fact the non-linearity observed in the current results is to be expected: as IWC increases, the scattering particles in the cloud become less efficient at directing radiation into the sensor LOS because of multiple scattering (the saturation effect). Therefore in a dense cloud, an increase in IWC results in a smaller increase in the observed radiance than it would do in a sparse cloud.

In fitting functions to the data, the shape of the plotted data, analysis of residuals, and assessment of the quality of fitted models were taken into account. All fitted models were assumed to pass through the origin. Allowing for a non-zero intercept made an insignificant difference to best-fit equations and error estimates. In most cases quadratic models appear most appropriate for both EOS SV and LOS SV IWC measurements. In cases where there was little to choose between linear and quadratic fits, the linear model was chosen for simplicity. It is clear from plots of T_{cir} against IWC that the data are heteroscedastic (i.e. the absolute error in IWC grows with T_{cir}) and this must be taken into account in the chosen regression model. The error in IWC was assumed to be proportional either to $\sqrt{T_{cir}}$ (100 hPa) or to T_{cir} (147 and 215 hPa) depending on the spread of the data. The following is an example quadratic model in which the error in IWC is assumed to be proportional to $\sqrt{T_{cir}}$. The simulated (T_{cir}, IWC) data points are assumed to satisfy

$$\text{IWC}_i = \beta_1 \cdot T_{cir,i} + \beta_2 \cdot T_{cir,i}^2 + \epsilon_i \cdot \sqrt{T_{cir,i}} \qquad (1)$$

where the subscript i denotes the sample number, and the errors $\epsilon_1, \ldots, \epsilon_n$ are independent and are distributed $N(0, \sigma^2)$. The value of σ is determined from the regression and the

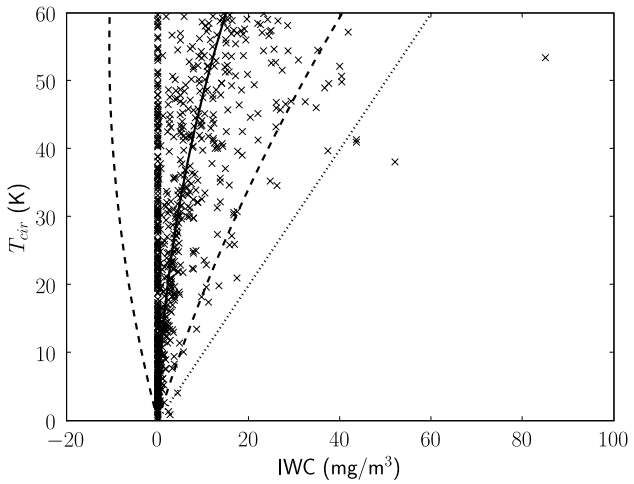

Fig. 5. Least-squares fit at 215 hPa for IWC in the EOS SV. The solid curve is the best-fit, the dashed curves are the 2-σ error bars. The dotted line represents the retrieval coefficient derived by Wu *et al.* [3].

product $\sigma \cdot \sqrt{T_{cir}}$ is an estimate of the standard deviation in the predicted IWC at the given T_{cir}.

In order to increase confidence in the assumptions regarding the variation of the error with T_{cir}, the data points were divided into bins of T_{cir} (for example: 0-2 K, 2-4 K, and so on) and the mean and standard deviation in IWC were calculated for each bin. These calculated errors were found to match the 2-σ regression errors well in most cases. They are also useful in providing estimated bounds on relative errors at small IWC since, under the assumption that the error grows as $\sqrt{T_{cir}}$, the estimated relative errors are unbounded as IWC approaches zero. Fig. 5 shows the fitted model at 215 hPa for EOS SV IWC.

B. EOS SV IWC

The fitted models for the EOS SV IWC are shown in Table II. The correlation coefficients are relatively low, especially at 215 hPa. This is due in part to the large number ($\sim$40% at 215 hPa) of samples with zero IWC and significant T_{cir} which occur when the LOS passes through the cloud while the sampling volume and cloud do not intersect.

The retrieval coefficients derived by Wu *et al.* (in units of mg/m^3 / K) decrease as tangent height altitude increases. In contrast, the opposite is observed in the simulated data here. This makes sense intuitively for a number of reasons. In the clear-sky case the observed radiance is directly related to the amount of ambient radiation at the tangent height of the observation. If ice particles are present then the sensor receives more radiation than for a clear-sky observation due to scattering and emission processes. At higher altitudes where the temperature is lower, a smaller proportion of the ice mass is composed of larger particles, which implies that there are fewer scattering particles at higher altitude for a given IWC. The lower temperature also results in less ambient radiation available to be scattered into the LOS. Furthermore, the ice particles themselves are colder and so emit less radiation. These factors mean that the T_{cir} (i.e. the radiance received by the sensor due to the ice particles, above and beyond the clear-sky radiance) is smaller at higher altitude for a given IWC.

Table II also shows the estimated 2-σ errors in IWC. Fig. 6 shows these plotted as relative errors in IWC at each tangent height for the EOS SV IWC. The relative errors decrease as IWC increases as a result of the quadratic (or linear) models and the assumption of the T_{cir}-dependence of the error in IWC: IWC grows as T_{cir}^2 (or as T_{cir}) while the error grows only as T_{cir} or as its square root.

For a number of the fitted models in this study, comparison of the estimated errors from the regression with the errors calculated from the binned data suggests that there is a tendency to over-estimate relative errors at small IWC (often due to the unbounded nature of the error model), and to under-estimate errors at larger IWC. Nevertheless, the errors estimated from the regressions provide useful estimates of the uncertainty in IWC retrievals based on the fitted functions, and the errors calculated directly from the data offer estimated bounds on uncertainty for low IWC. For example, at 100 hPa a visual inspection of the data suggests the 2-σ error is only around 100-150% for $1 <$ IWC < 5 mg/m^3. This is supported by calculation of the standard deviation in the binned data over this range as shown in Fig. 6. At 215 hPa the error is also large for small IWC (though errors linear in T_{cir} are in fact bounded as IWC approaches zero). However, calculation of the mean and standard deviation of the data at small IWC suggests the error is around 300-350% for $1 <$ IWC < 4 mg/m^3.

Fig. 6 also shows the estimated errors in EOS MLS IWC quoted in [19] which are based on comparisons with CloudSat IWC retrievals. These are specified separately for IWC $<$ 10 mg/m^3 and IWC $>$ 10 mg/m^3. At 100 hPa the error appears considerably lower than the quoted value for IWC $>$ 10 mg/m^3. At 147 hPa the relative error is broadly comparable with the estimate from the CloudSat comparisons. The 215 hPa error appears somewhat larger than the CloudSat estimate for higher IWC. The results also suggest that at the two lower tangent height altitudes (215 and 147 hPa), the maximum values of IWC that can be predicted with reasonable accuracy are considerably smaller than the 50 mg/m^3 quoted in [19].

The relative error at 215 hPa is very much larger than at the two higher altitudes for any given IWC. Various factors contribute to this such as the greater range of IWC values found at lower altitudes due to the exponential variation of IWC with temperature, which results in a wider range of IWC values which may yield any given T_{cir}. It may also be related to the relative length of the sampling volume along the LOS compared to the path length of the LOS within the troposphere. This path length covers the portion of the FOV along which clouds may be found in any given observation. If the sampling volume accounts for a smaller proportion of it, one may expect larger uncertainties due to the effect of ice mass which is outside the sampling volume, but still within the FOV. Simple geometry shows that at 215 hPa the sampling volume accounts for $\sim$55% of this tropospheric path length, while at 147 hPa it is $\sim$67%, and at 100 hPa, $\sim$63%. These values correspond to the sizes of the relative errors at each tangent height (147 hPa having the smallest error, and 215

TABLE II
LEAST-SQUARES FITTED EQUATIONS AND ERROR ESTIMATES FOR IWC-T_{cir} RELATIONS WITH THE MH97 PSD

SV	Pressure (hPa)	Model IWC (mg/m^3)	r	Maximum T_{cir} (K)	Maximum IWC (mg/m^3)	σ (mg/m^3)	2-σ error (mg/m^3)
EOS	215	$0.0382T_{cir} + 0.0035T_{cir}^2$	0.558	60	15	0.212	$\pm 0.424T_{cir}$
	147	$0.218T_{cir} + 0.0047T_{cir}^2$	0.773	60	30	0.202	$\pm 0.404T_{cir}$
	100	$0.616T_{cir}$	0.834	80	49	1.31	$\pm 2.62\sqrt{T_{cir}}$
LOS	215	$0.0136T_{cir} + 0.0041T_{cir}^2$	0.635	60	16	0.137	$\pm 0.274T_{cir}$
	147	$0.0938T_{cir} + 0.0052T_{cir}^2$	0.860	60	24	0.105	$\pm 0.210T_{cir}$
	100	$0.440T_{cir} + 0.0025T_{cir}^2$	0.862	80	51	1.05	$\pm 2.10\sqrt{T_{cir}}$

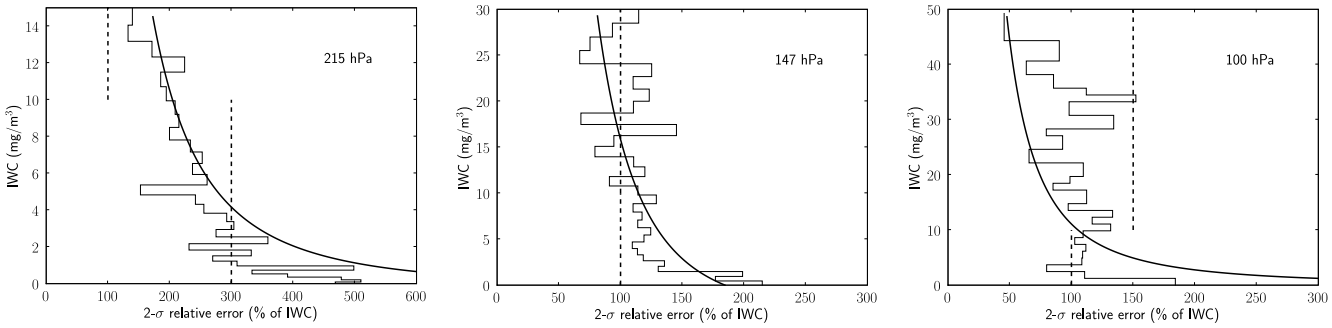

Fig. 6. The curves show the 2-σ relative errors in EOS SV IWC at 215, 147 and 100 hPa based on regression analysis. The stepped lines show the relative error as calculated from the mean and standard deviation of the data grouped into T_{cir} bins. Dashed lines are the errors estimated from comparison with CloudSat IWC retrievals [19]. These are specified for IWC $<$ 10 mg/m^3 and IWC $>$ 10 mg/m^3 up to a maximum of 50 mg/m^3.

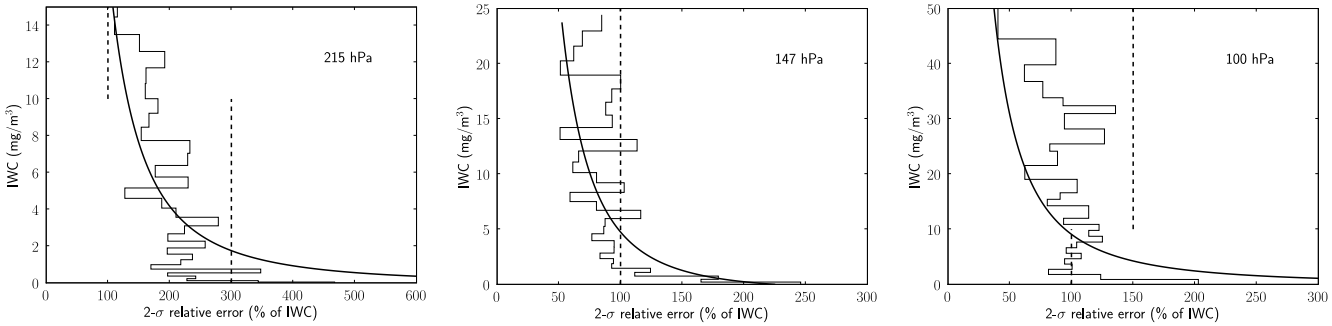

Fig. 7. The curves show the 2-σ relative errors in LOS SV IWC at 215, 147 and 100 hPa. The dashed and stepped lines are as in Fig. 6. The estimated errors from comparison with CloudSat IWC are shown for reference, but they refer to IWC over the EOS SV rather than the LOS SV.

hPa the largest). The influence on measured radiance of ice mass outside the sampling volume depends on the PSD, since these regions are higher (and so colder) than the sampling volume, and will typically contain a smaller proportion of larger, scattering particles.

These errors represent the estimated uncertainty in EOS MLS IWC retrievals due to variability of cloud geometry and cloud-sensor position under the assumption of a particular particle size distribution (MH97). Results of simulations using alternative PSDs are discussed in section V.

C. LOS SV IWC

Table II also contains the fitted models for the LOS SV IWC, and Fig. 7 shows the corresponding relative errors. Similar comments apply to these models as for the EOS SV ones. However, the results suggest that the average IWC within the LOS SV can be retrieved with considerably greater accuracy than the IWC within the EOS SV, particularly at lower tangent heights. Comparison of the relative errors shows LOS SV IWC uncertainty to be around 10% smaller at 100 hPa, up to 35% smaller at 147 hPa, and more than 60% smaller at 215 hPa. Under the LOS SV definition there are fewer zero IWC values at lower tangent heights (especially 215 hPa) than for the EOS SV due to the geometry of the measurements as described in Section III. This is part of the reason that the difference in the errors between the two sampling volume definitions is greatest at 215 hPa.

The difference in the errors is also a result of the difference in the relative contributions made to T_{cir} by the ice mass within each sampling volume. This is governed by the interplay between the sensor sensitivity pattern, and the variations in the particle size distribution and IWC over the sampling volume. The further away ice particles are from the LOS, the smaller their contribution due to the sensor response function. There will typically be a greater contribution to the observed radiance from particles towards the bottom of the

sampling volume than the top due to the fact that IWC varies exponentially with temperature, and also because there are more large (scattering) particles in warmer regions according to the PSD. The error in IWC will be smaller for the sampling volume which contains the ice mass which makes the greatest contribution to T_{cir} as determined by these various factors. In this case it appears that the ice mass with the most influence on T_{cir} is contained within the LOS SV. However, it will be seen in the next section that this may not be the case if an alternative PSD is assumed.

V. Particle Size Distribution

The simulations discussed so far assumed the MH97 PSD. As mentioned in Section II the choice of PSD has considerable influence on the modelled T_{cir}-IWC relationship: along with horizontal inhomogeneity and the cloud-sensor geometry, it is one of the largest factors contributing to uncertainty in IWC retrievals. Results are presented here for simulations using two alternative size distributions to MH97.

A. Mitchell et al. 1999

M99 comprises a sum of two exponential distributions accounting for small and large particles, distinguished by having maximum dimension less than or greater than 100 μm. The M99 distribution depends only on temperature and assumes particles are planar polycrystals. For the simulations, spherical particles of mass-equivalent radius were used. The transformation from polycrystals to mass-equivalent spheres is described in [20]. Fig. 8 compares MH97 and M99 for a range of values of IWC and temperature. In general, large particles constitute a considerably smaller proportion of total ice mass in M99 than MH97. Fewer scattering particles mean that for a particular IWC, the resulting observed radiance is smaller with M99 than with MH97. This also means that the saturation effect is not clearly in evidence so that reasonably accurate (up to the assumption of size distribution) retrievals are possible over a wider range of IWC values, much larger than the maximum of 50 mg/m^3 quoted in [19]. At the higher tangent heights the saturation effect was not observed in the randomised scenarios, so an upper limit on retrievable IWC was not obtained. It is also noteworthy that as temperature decreases, the proportion of large particles in the M99 distribution drops sharply: at higher altitudes there are significantly fewer scattering particles. Table III lists the fitted models and errors for EOS SV and LOS SV IWC.

Fig. 9 shows the estimated errors in EOS SV IWC. The estimated uncertainties in IWC retrievals due to geometrical factors are smaller with M99 than with MH97. This is probably due to the sharp drop in density of large particles as temperature decreases with the M99 size distribution. Any ice mass within the FOV which lies outside the sampling volume comprises a smaller proportion of large particles than ice mass within the sampling volume as a result of it being significantly higher (and thus colder) than the tangent point. This ice mass therefore contributes much less to the observed radiance than the ice within the sampling volume. As a result, T_{cir} is most

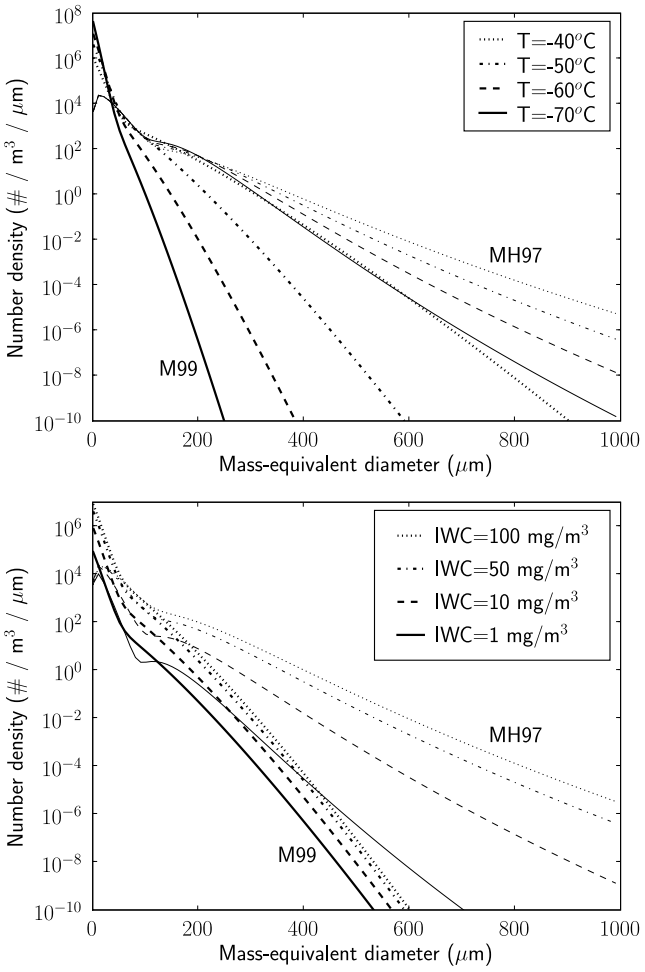

Fig. 8. M99 (thick lines) and MH97 (thin lines) particle size distributions. Top: IWC is 50 mg/m^3 and temperature varies. Bottom: temperature is $-50\,^\circ$C and IWC varies. The M99 distribution comprises significantly fewer large particles compared to MH97, especially at lower temperatures.

sensitive to ice within the sampling volume, and much less sensitive to particles outside this volume than with MH97.

Note also that the observations for which the IWC is zero all have low T_{cir} because of the small effect that ice mass outside the sampling volume has on observed radiance. Thus the uncertainty in observations at 215 hPa (where zero IWC measurements are most common) is not so much larger than the uncertainty at higher tangent heights as compared with the results for MH97.

The fitted models for M99 are significantly different to those for MH97 at each tangent height. This implies that where the size distribution is unknown, the uncertainty in the IWC associated with a given T_{cir} due to PSD may be very much greater than the uncertainty due to geometrical factors. Fig. 10 plots the predicted IWC for M99 divided by that for MH97 for the range of T_{cir} over which the regressions apply at each tangent height. The choice of PSD can alter the retrieved IWC by a factor of between 3 and 8 depending on tangent height and T_{cir}. The uncertainty grows larger with increasing tangent height since at higher altitudes the two PSDs differ more markedly in terms of the proportion

TABLE III
LEAST-SQUARES FITTED EQUATIONS AND ERROR ESTIMATES FOR IWC-T_{cir} RELATIONS WITH THE M99 PSD

SV	Pressure (hPa)	Model IWC (mg/m^3)	r	Maximum T_{cir} (K)	Maximum IWC (mg/m^3)	σ (mg/m^3)	2-σ error (mg/m^3)
EOS	215	$0.117T_{cir} + 0.0131T_{cir}^2$	0.967	85	105	0.979	$\pm 1.96\sqrt{T_{cir}}$
	147	$1.00T_{cir} + 0.0244T_{cir}^2$	0.978	>60	>148	1.40	$\pm 2.80\sqrt{T_{cir}}$
	100	$3.29T_{cir} + 0.0867T_{cir}^2$	0.979	>17	>81	1.81	$\pm 3.62\sqrt{T_{cir}}$
LOS	215	$0.223T_{cir} + 0.0116T_{cir}^2$	0.971	85	100	0.976	$\pm 1.95\sqrt{T_{cir}}$
	147	$0.823T_{cir} + 0.0206T_{cir}^2$	0.954	>60	>124	1.71	$\pm 3.42\sqrt{T_{cir}}$
	100	$2.62T_{cir} + 0.114T_{cir}^2$	0.976	>17	>78	1.55	$\pm 3.10\sqrt{T_{cir}}$

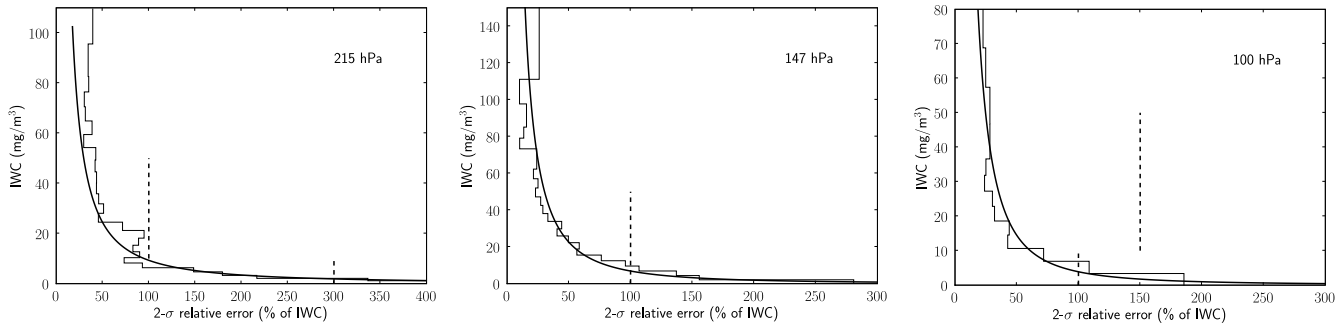

Fig. 9. The curves show the 2-σ relative errors in EOS SV IWC with the M99 PSD at 215, 147 and 100 hPa. The dashed and stepped lines are as in Fig. 6.

of the ice mass comprising large particles. At 215 hPa the difference corresponds to 200-250% of the MH97 IWC which is comparable with the uncertainty in the MH97 retrievals due to geometrical factors at this tangent height. At 147 hPa the difference in IWC between the PSDs is 350-400% of the MH97 IWC, and at 100 hPa it is 450-700%. Clearly then, at the higher tangent heights the uncertainty due to PSD is potentially much greater than the uncertainty due to cloud geometry.

Under this particle size distribution, the uncertainties in IWC retrievals over the LOS SV are approximately the same as for the EOS SV at 100 and 215 hPa. At 147 hPa, the error in LOS SV IWC is approximately 5-30% larger (the difference grows as IWC decreases). Under this PSD it appears therefore that T_{cir} is slightly better at predicting the IWC within the EOS SV than the LOS SV.

A comparison of the LOS SV IWC predicted with the M99 and MH97 distributions (Fig. 10) shows that the uncertainty due to PSD is larger than that for EOS SV IWC. The difference at the two lower tangent heights for small radiance is much larger. It appears that the T_{cir}-IWC relationship for the EOS SV is more stable than that for the LOS SV under alternative parameterisations of particle sizes.

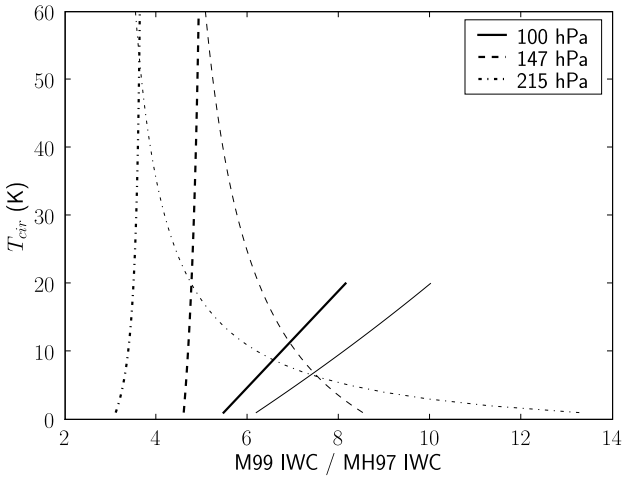

Fig. 10. Predicted EOS SV (thick lines) and LOS SV (thin lines) IWC for M99 divided by those for MH97 against T_{cir}. The retrieved IWC for a measured radiance depends strongly on the assumed PSD.

B. Heymsfield 2003

Simulations were also carried out with the unimodal gamma distribution described by Heymsfield [11]. The number density N is given by

$$N = N_0 D^{\mu} e^{-\lambda D} \tag{2}$$

where D is the maximum particle dimension, μ is the dispersion of the distribution, λ is the slope, and N_0 is the intercept. In the simulations, the parameters λ and μ were randomised according to

$$\lambda = 20.25 e^{-0.042 T_C + \epsilon_\lambda} \tag{3}$$

where T_C is the temperature in Celsius and ϵ_λ is distributed $N(0, 0.5)$, and

$$\mu = 0.076\lambda^{0.8} - 2 + \epsilon_\mu \tag{4}$$

where ϵ_μ is distributed $N(0, 0.01)$. The temperature dependence of λ is defined separately for temperatures above and below $-18\,^{\circ}$C in [11], but for these simulations all temperatures were lower than this. The parameters were chosen randomly according to the above distributions at each grid point within the cloud, and N_0 was set so as to match the specified local IWC. These distributions were obtained experimentally

TABLE IV
LEAST-SQUARES FITTED EQUATIONS AND ERROR ESTIMATES FOR IWC-T_{cir} RELATIONS WITH THE H03 PSD

SV	Pressure (hPa)	Model IWC (mg/m^3)	r	Maximum T_{cir} (K)	Maximum IWC (mg/m^3)	σ (mg/m^3)	2-σ error (mg/m^3)
EOS	147	$0.388T_{cir}$	0.346	45	17	0.418	$\pm 0.836T_{cir}$
	100	$0.405T_{cir}$	0.482	55	22	0.391	$\pm 0.782T_{cir}$
LOS	147	$0.219T_{cir}$	0.377	45	10	0.264	$\pm 0.528T_{cir}$
	100	$0.301T_{cir}$	0.519	55	17	0.302	$\pm 0.604T_{cir}$

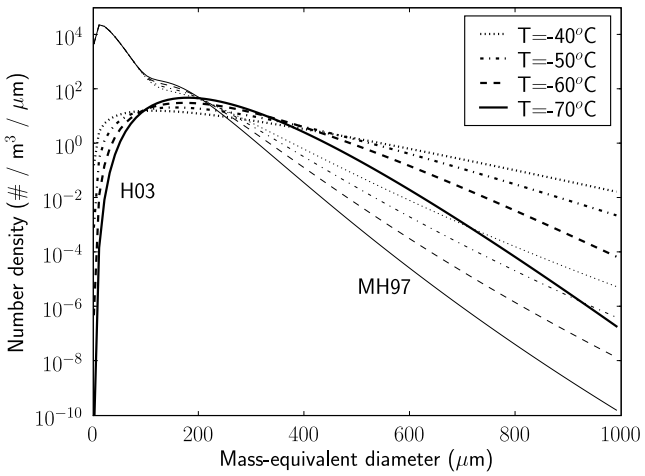

Fig. 11. Mean H03 (thick lines) and MH97 (thin lines) particle size distributions. IWC is 50 mg/m^3. Note that the H03 distribution varies considerably from the mean shape shown here under the randomisation scheme employed.

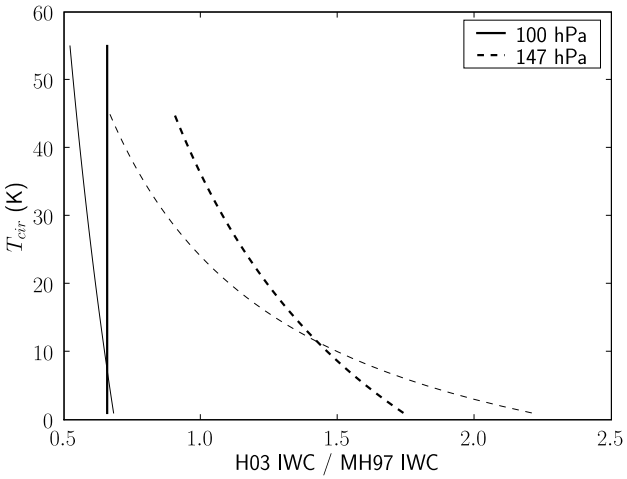

Fig. 13. Predicted EOS SV (thick lines) and LOS SV (thin lines) IWC for H03 divided by those for MH97 against T_{cir}.

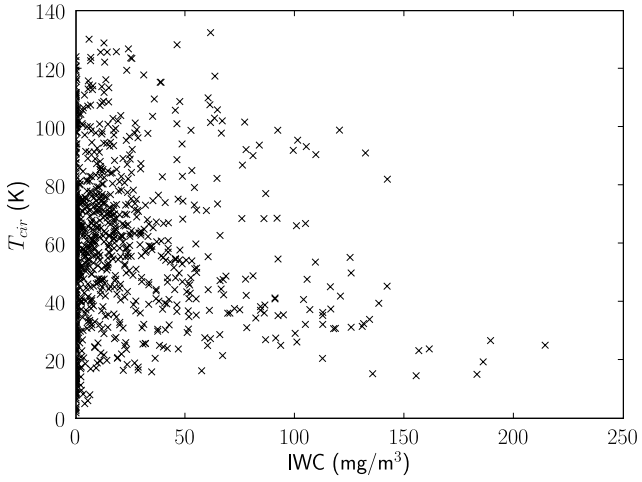

Fig. 12. T_{cir} against EOS SV IWC with the H03 PSD at 215 hPa. Retrieving IWC from T_{cir} with reasonable accuracy is not possible due to the saturation effect.

to match Heymsfield's results. The mean H03 distribution for various temperatures is compared to MH97 in Fig. 11. Large particles often constitute a greater proportion of these distributions than MH97, though for some values of λ and μ the proportion can be smaller. From this it is expected that saturation would occur more readily than with MH97, and such is found to be the case. In fact saturation occurs for $T_{cir} > 14$ K at 215 hPa (Fig. 12) which prevents meaningful retrievals of IWC at this tangent height. Of the $\sim$1000 data points generated at this tangent height, only 38 had radiances less than 14 K (most of them with zero IWC), and the IWC corresponding to 14 K appears to be of the order of 1 or 2 mg/m^3.

Table IV shows fitted models for the other two tangent heights. The correlation coefficients are very low as a result of the large spread of values. It is not obvious which is the best model to fit to the data, but a linear model with error proportional to T_{cir} appears to characterise the error reasonably well. This model implies that relative errors are constant with respect to IWC.

The EOS SV IWC error is 215% at 147 hPa and 193% at 100 hPa, which are generally larger than the errors obtained with the other two PSDs, except at very small IWC (of order a few mg/m^3). This is probably due to the randomised particle distribution: scenarios are generated in which the proportion of the ice mass consisting of large particles may either be larger or smaller than that for MH97. There is therefore a wider range of IWC values which may yield any particular T_{cir} than for MH97. Furthermore, in cases where the density of scattering particles is higher than for MH97, the ice mass outside the sampling volume may have a significant impact on the observed radiance while not being accounted for in the IWC measure, which also increases the variance in IWC as discussed previously. Fig. 13 compares the retrieved IWC for H03 and MH97: they differ by a factor of less than two. The difference corresponds to less than 80% of the predicted

MH97 IWC at all T_{cir}, which is of comparable size to the geometrical errors in IWC with MH97.

With this distribution the LOS SV IWC error due to geometrical factors is 241% at 147 hPa and 201% at 100 hPa. These are 25% and 10% larger than the respective EOS SV IWC errors suggesting that, as for M99, T_{cir} is a better predictor of EOS SV IWC than LOS SV IWC under the H03 size distribution.

Comparison with LOS SV IWC retrievals using MH97 are also shown in Fig. 13. As with M99 and MH97, the difference between H03 and MH97 retrievals is generally greater than for EOS SV IWC. Once again it appears that the T_{cir}-IWC relationship for IWC over the EOS SV is the more stable under the assumption of this alternative PSD.

As may be anticipated, it appears that the randomisation of the PSD increases the uncertainty in the IWC retrievals as a result of the sensitivity of the observed radiance to the number of scattering particles. Since variability would naturally be expected in the distribution of particle sizes around the assumed PSD, the true errors in retrievals under the assumption of the MH97 and M99 PSDs are very likely to be larger than the estimates presented above since such variability was not taken into account in those simulations.

VI. Retrieval of Ice Mass

Ice particles along the entire LOS contribute to the observed radiance, but the size of the contribution depends on how the PSD varies within the FOV. If the proportion of large particles drops rapidly with temperature (as for M99), there will be relatively few scattering particles in any cloud found towards the extremities of the FOV (i.e. away from the tangent point), and so these particles will contribute little to the observed radiance. Alternative parameterisations of particle size (such as MH97 and H03) predict larger proportions of scattering particles in these regions resulting in larger contributions to T_{cir}. This section addresses the question of whether the uncertainty in ice mass measurements over the entire FOV is smaller than that in IWC measurements over a sampling volume.

A similar analysis to that for IWC was applied to the total ice mass within the FOV along the entire LOS for each of the three particle size distributions. Table V lists the fitted functions and the estimated errors. In most cases the same models were used as for the LOS SV IWC, the exceptions being two tangent heights with M99 where cubic models appeared more suitable. With MH97 and M99, the errors are approximately proportional to $\sqrt{T_{cir}}$ at all tangent heights. The saturation effect typically occurs at the same radiance values as for IWC, so in most cases the same T_{cir} cut-off was used as for the corresponding IWC relation.

Assuming MH97, the errors in ice mass retrievals are substantially smaller than those for IWC. At 215 hPa, the errors in ice mass are smaller than the LOS SV IWC errors by about 50-100%, while at 147 and 100 hPa they are smaller by about 25% and roughly 15-40% respectively. However, with the M99 PSD, the ice mass errors at 215 hPa are 15-40% larger than LOS SV IWC errors for T_{cir} above ∼20 K. At 147 and 100 hPa, ice mass errors are about 25% and 5% larger respectively.

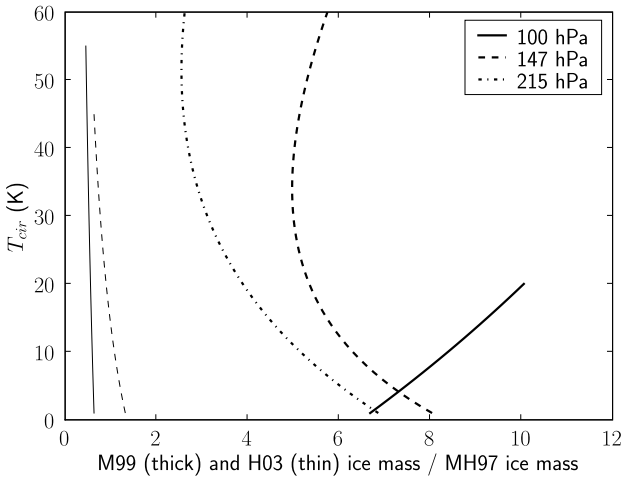

Fig. 14. Predicted ice mass for M99 (thick lines) and for H03 (thin lines) divided by that for MH97 against T_{cir}.

So under the assumption of MH97, ice mass errors are smaller than IWC errors, suggesting ice mass outside the sampling volume has a significant effect on observed radiances, and that errors are reduced if it is taken into account. However, if M99 is assumed, IWC errors are generally smaller than ice mass errors, suggesting ice mass outside the sampling volume has a small impact on observed radiances and so more accurate measurements are made if only the ice mass within the sampling volume is accounted for.

With H03, the ice mass error is 220% at 147 hPa and 179% at 100 hPa. As with IWC, the randomised size distribution results in a wide spread of FOV ice masses which can yield any particular T_{cir}. The result is that these errors are generally larger than those for the other two size distributions. The uncertainties in ice mass are about 20% smaller than for LOS SV IWC, and approximately the same size as the errors in EOS SV IWC (5% more at 147 hPa and 10% less at 100 hPa). Since the H03 distributions often involve a greater proportion of large particles than MH97, one might expect the errors in ice mass to be smaller than those in IWC since the ice mass outside the sampling volume will influence the observed radiances to a larger extent. The fact that the errors in ice mass and IWC with H03 are quite similar suggests that the error resulting from the randomised PSD may dominate the error due to accounting (or not) for ice mass outside the sampling volume.

The potential error due to PSD is illustrated in Fig. 14. Comparing retrieved ice mass with MH97 and M99, the difference in retrieved values is generally larger than that for EOS SV IWC. Comparing H03 and MH97, the difference is similar to that for IWC. So the potential error due to PSD may be greater for ice mass retrievals than for EOS SV IWC retrievals, while it is broadly comparable to that for LOS SV IWC retrievals.

The results indicate that the total ice mass within the instrument FOV may be retrieved from measurements of cloud-

TABLE V
LEAST-SQUARES FITTED EQUATIONS AND ERROR ESTIMATES FOR ICE MASS-T_{cir} RELATIONS

PSD	Pressure (hPa)	Model ice mass (kg)	r	Max. T_{cir} (K)	Max. ice mass (10^6 kg)	σ (10^6 kg)	2-σ error (10^6 kg)
MH97	215	$1.85 \times 10^6 T_{cir} + 2.43 \times 10^4 T_{cir}^2$	0.764	60	198	7.43	$\pm 14.9\sqrt{T_{cir}}$
	147	$1.47 \times 10^6 T_{cir} + 3.72 \times 10^4 T_{cir}^2$	0.927	60	222	3.88	$\pm 7.76\sqrt{T_{cir}}$
	100	$3.95 \times 10^6 T_{cir} + 2.92 \times 10^4 T_{cir}^2$	0.924	80	503	6.56	$\pm 13.1\sqrt{T_{cir}}$
M99	215	$1.31 \times 10^7 T_{cir} - 2.65 \times 10^5 T_{cir}^2 + 3.18 \times 10^3 T_{cir}^3$	0.948	>100	>2000	20.1	$\pm 40.2\sqrt{T_{cir}}$
	147	$1.23 \times 10^7 T_{cir} - 1.04 \times 10^5 T_{cir}^2 + 4.25 \times 10^3 T_{cir}^3$	0.914	>60	>1280	22.9	$\pm 45.7\sqrt{T_{cir}}$
	100	$2.56 \times 10^7 T_{cir} + 9.99 \times 10^5 T_{cir}^2$	0.975	>17	>724	16.7	$\pm 33.4\sqrt{T_{cir}}$
H03	147	$1.99 \times 10^6 T_{cir}$	0.412	45	89.6	2.19	$\pm 4.38 T_{cir}$
	100	$2.52 \times 10^6 T_{cir}$	0.579	55	139	2.25	$\pm 4.51 T_{cir}$

induced radiance. The errors in retrievals due to geometrical factors may be smaller than those for IWC, but the difference depends on the assumed PSD since this determines the extent to which ice mass towards the extremities of the FOV contributes to the observed radiance. However, the potential error in total ice mass due to uncertainty in the PSD may exceed that for IWC retrievals over the EOS SV.

VII. SUMMARY

This paper describes simulations of EOS MLS IWC measurements and presents an analysis of the uncertainty in the retrievals. The simulations were randomly generated with parameters determined on the basis of observations of tropical cirrus clouds. The estimated errors in EOS MLS IWC retrievals due to horizontal inhomogeneity and cloud-sensor geometry are presented. At 147 hPa, the errors are found to be of similar size to estimated errors from comparison with CloudSat IWC measurements, and at 100 and 215 hPa, the errors are found to be respectively less than and greater than the Cloudsat estimated errors for values of IWC above $\sim$10 mg/m^3. The results also suggest that at lower tangent heights the maximum value of IWC which can be retrieved with reasonable accuracy is smaller than the 50 mg/m^3 quoted in [19].

The effect of assuming alternative PSDs has been investigated and it is found that the error due to uncertainty in the PSD is potentially very large indeed at higher tangent heights. At 215 hPa, it is of the same order of magnitude as the error due to geometrical factors. However, it is not possible to retrieve IWC from T_{cir} measurements at 215 hPa with the H03 PSD due to the saturation effect. The error due to PSD may be reduced if the size distribution in the clouds being observed can be more accurately characterised. This might be achieved using observations at multiple frequencies: it has been found that measurements from the 240 and 640 GHz EOS MLS radiometers may be combined to obtain information about the PSD [3]. For the simulations using the H03 distribution, the PSD was randomised. The uncertainties in IWC retrievals with this PSD are typically larger than with the other two, and this is very probably in part a result of the randomisation of the PSD. This indicates that the estimated errors obtained using the MH97 and M99 distributions may under-estimate the true uncertainties in IWC since natural variability in the assumed PSD was not accounted for in those simulations.

Employing an alternative definition of the volume over which the retrieved IWC applies results in considerably smaller uncertainties with MH97. For example, relative errors in LOS SV IWC are more than 60% smaller than for EOS SV IWC at 215 hPa. However, under the M99 and H03 PSDs, the uncertainties in LOS SV IWC are at best equal with and in some cases worse than those in EOS SV IWC (in the worst case, the relative error is up to $\sim$30% larger at 147 hPa with M99). The results therefore suggest that the uncertainty may be reduced by retrieving IWC over an alternative sampling volume, but this depends on the assumed PSD.

The error in IWC due to PSD is found to be larger with IWC over the LOS SV than with the EOS SV IWC, especially for small T_{cir} at 215 and 147 hPa. The relationship between T_{cir} and IWC appears more stable under alternative PSD parameterisations for IWC defined over the EOS SV compared to IWC in the LOS SV.

It is found that total ice mass within the FOV may be retrieved from cloud-induced radiance measurements with smaller uncertainty than IWC under the assumption of the MH97 PSD (the relative error in ice mass is up to $\sim$100% smaller than that in LOS SV IWC at 215 hPa). Once again, this depends on the assumed PSD: with M99 the uncertainties in ice mass are larger than those for IWC (up to $\sim$40% larger at 215 hPa). Ice mass is therefore another quantity which may be retrieved from EOS MLS measurements of high altitude clouds. However, the potential error due to PSD is significantly larger for ice mass than for EOS SV IWC retrievals when comparing the M99 and MH97 distributions. The PSD-related error in ice mass is broadly comparable to that in LOS SV IWC.

This study has quantitatively analysed the errors in EOS MLS IWC retrievals due to horizontal inhomogeneity of clouds and relative positioning of cloud and sensor. The uncertainty due to assumed PSD has also been investigated. It is hoped that the contribution this brings to the understanding of the errors in IWC retrievals may be useful in constraining cloud parameters in GCMs, and hence in improving accuracy of climate models.

ACKNOWLEDGMENT

The first author would like to thank Dr Cory Davis and Dr Hugh Pumphrey for providing helpful advice, and also the Natural Environment Research Council who provided funding

throughout his Master's degree for which this research was undertaken.

REFERENCES

[1] K. N. Liou, "Influence of cirrus clouds on weather and climate processes: a global perspective," *Mon. Wea. Rev.*, vol. 114, pp. 1167–1199, 1986.

[2] G. L. Stephens, S. C. Tsay, P. W. Stackhouse, Jr., and P. J. Flateau, "The relevance of the microphysical and radiative properties of cirrus clouds to climate and climatic feedback," *J. Atmos. Sci.*, vol. 47, pp. 1742–1753, 1990.

[3] D. L. Wu, J. H. Jiang, and C. P. Davis, "EOS MLS cloud ice measurements and cloudy-sky radiative transfer model," *IEEE Trans. Geosci. Remote Sens.*, vol. 44, no. 5, pp. 1156–1165, 2006.

[4] J.-L. Li *et al.*, "Comparisons of EOS MLS cloud ice measurements with ECMWF analyses and GCM simlations: initial results," *Geophys. Res. Lett.*, vol. 32, 2005, l18710, DOI:10.1029/2005GL023 788.

[5] D. R. Dowling and L. R. Radke, "A summary of the physical properties of cirrus clouds," *J. Appl. Meteor.*, vol. 29, pp. 970–978, 1990.

[6] S. A. Buehler, P. Eriksson, T. Kuhn, A. von Engeln, and C. Verdes, "ARTS, the atmospheric radiative transfer simulator," *J. Quant. Spectrosc. Radiat. Transf.*, vol. 91, no. 1, pp. 65–93, 2005.

[7] C. P. Davis, C. Emde, and R. Harwood, "A 3-D polarised reversed monte carlo radiative transfer model for millimetre and sub-millimetre passive remote sensing in cloudy atmospheres," *IEEE Trans. Geosci. Remote Sens.*, vol. 43, no. 5, pp. 1096–1101, 2005.

[8] A. Baran, "On the scattering and absorption properties of cirrus cloud," *J. Quant. Spectrosc. Radiat. Transf.*, vol. 89, pp. 17–36, 2004.

[9] G. M. McFarquhar and A. J. Heymsfield, "Parameterization of tropical cirrus ice distributions and implications for radiative transfer: results from CEPEX," *J. Atmos. Sci.*, vol. 54, pp. 2187–2200, 1997.

[10] D. L. Mitchell, D. Ivanova, J. M. Edwards, and G. C. McFarquhar, "A GCM parameterization of bimodal size spectra for ice clouds," in *Ninth ARM Science Team Meeting Proceedings*, San Antonio, Texas, Mar. 1999.

[11] A. J. Heymsfield, "Properties of tropical and midlatitude ice cloud particle ensembles. part II: Applications for mesoscale and climate models," *J. Atmos. Sci.*, vol. 60, pp. 2592–2611, 2003.

[12] S. T. Bond, "The potential effect of cirrus on Microwave Limb Sounder retrievals," Ph.D. dissertation, Univ. of Edinburgh, Edinburgh, U.K., 1996.

[13] A. J. Heymsfield and C. M. R. Platt, "A parameterisation of the particle size spectrum of ice clouds in terms of the ambient temperature and the ice water content," *J. Atmos. Sci.*, vol. 41, no. 5, pp. 846–855, 1984.

[14] A. J. Heymsfield and G. M. McFarquhar, *Cirrus*. Oxford, UK: Oxford: Oxford University Press, 2002, ch. 4.

[15] G. P. Anderson *et al.*, "AFGL atmospheric constituent profiles (0 - 120 km)," Air Force Geophysics Laboratory, Tech. Rep. TR-86-0110, 1986.

[16] W. Haag *et al.*, "Freezing thresholds and cirrus cloud formation mechanisms inferred from in situ measurements of relative humidity," *Atmos. Chem. Phys.*, vol. 3, pp. 1791–1806, 2003.

[17] R. E. Cofield and P. C. Stek, "Design and field-of-view calibration of 114-660-GHz optics of the Earth Observing System Microwave Limb Sounder," *IEEE Trans. Geosci. Remote Sens.*, vol. 44, no. 5, pp. 1166–1181, 2006.

[18] R. F. Jarnot, V. S. Perun, and M. J. Schwartz, "Radiometric and spectral performance and calibration of the GHz bands of EOS MLS," *IEEE Trans. Geosci. Remote Sens.*, vol. 44, no. 5, pp. 1131–1143, 2006.

[19] N. J. Livesey *et al.*, "Version 2.2 level 2 data quality and description document," 2007, accessed 9 August 2007. [Online]. Available: http://mls.jpl.nasa.gov/data/v2-2_data_quality_document.pdf

[20] B. Rydberg, "Submillimeter-wave radiometric measurements of cirrus cloud ice," Master's thesis, Chalmers University of Technology, Goteborg, Sweden, 2004.